Forming Limits of Metal Sheets and Tubes: Analysis Method and Experimental Validation

Toshihiko Kuwabara [1,a], Kengo Yoshida [2,b] and Fuminori Sugawara [3,c]

[1] Division of Advanced Mechanical Systems Engineering, Institute of Engineering, Tokyo University of Agriculture and Technology, 2-24-16 Naka-cho, Koganei, Tokyo 184-8588, Japan

[2] Graduate School of Science and Engineering, Yamagata University, 4-3-16 Jonan, Yonezawa, Yamagata 992-8510, Japan

[3] Department of Mechanical Systems Engineering, Graduate School of Engineering, Tokyo University of Agriculture and Technology, 2-24-16 Naka-cho, Koganei, Tokyo 184-8588, Japan

[a] kuwabara@cc.tuat.ac.jp, [b] yoshida@yz.yamagata-u.ac.jp, [c] 50011833003@st.tuat.ac.jp

Keywords: strain localization, forming limit curve, yield function, crystal plasticity, biaxial tensile test

Abstract. In the first part of the paper, an analysis of strain localization phenomenon in a polycrystalline sheet is demonstrated on the basis of Marciniak and Kuczyński-type imperfection approach. A thin sheet which possesses a band-type initial thickness imperfection is considered, and biaxial stretching is applied to the rolling and transverse directions of the sheet. Hence, plane stress condition with zero thickness stress is assumed. The development of strain concentration into the band is numerically analyzed. Plotting strain levels at the onset of strain localization on strain space, stretchability of the sheet is represented as a forming limit curve (FLC). Firstly, a phenomenological plasticity theory is adopted in the simulation. The influence of material parameters, such as curvature of yield surface, magnitude of initial imperfection, strain-rate sensitivity, work-hardening exponent, and anisotropy is investigated. Secondly, a crystal plasticity theory based on a slip mechanism of plastic deformation is employed, and influence of typical textures generated in the rolling and recrystalization processes of aluminum alloy sheet production is examined.
In the second part of the paper, the experimental methods for determining the FLC and forming limit stress curve (FLSC) of sheet and tubular specimens are presented. For sheet specimens a biaxial stretch test using a flat-head punch proposed by Marciniak and Kuczyński is used. For tubular specimens a multiaxial tube expansion test is used; combined axial force and internal pressure are simultaneously applied to a tubular specimen using a closed loop, servo-controlled biaxial stress testing machine. The latter can be utilized as a biaxial tensile testing method for sheet metals by fabricating a tubular specimen from a flat sheet sample, and that it is even useful to measure the forming limits for nonlinear loading paths. Measured results of FLC and FLSC are presented and the calculated results based on the phenomenological and polycrystal plasticity analyses are validated. The strain path dependency of FLSC is also discussed.

Introduction

In a biaxially stretched sheet metal, the sheet deforms almost homogeneously up to a certain strain level, after which plastic deformation starts to localize into a narrow band region with significant reduction of the thickness and a localized neck is formed. Shortly after, a band with highly localized shear strains emerges in the neck, and is subsequently accompanied by the growth and coalescence of voids, finally leading to fracture. Thus, the onset of the localized neck plays the role of a precursor to breakage in sheet metals. In the present paper, we concentrate our attention on the

analysis of localized necking in sheets or thin-walled tubes subjected to plane-stress states. The present papare is constructed on the basis of our recent numerical and experimental investigations [1]-[6].

One of the first theoretical studies on localized necking was initiated by Hill [7], who treated the onset of localized necking as bifurcation from the homogeneous strain field to the highly localized deformation mode. A discontinuity in the velocity gradient was analyzed with the constraint of zero extension along the neck. There is, however, no line of zero extension in a biaxially stretched sheet, and hence Hill's formulation does not predict the onset of localized neck in the biaxial-stretching range. Marciniak and Kuczyński [8] developed a model in which a sheet is postulated to have a band-type initial thickness imperfection. They were able to predict limit strains in the biaxial-stretching range by analyzing the growth of the thickness imperfection. Following the direction of Hill, a framework of bifurcation analysis, which is capable of predicting the onset of localized neck in biaxially stretched sheets, was developed by Stören and Rice [9]. Both the imperfection analysis of Marciniak and Kuczyński and the bifurcation analysis of Stören and Rice have been well accepted and widely used for forming limit analyses of sheet metals. Whether the preexistence of initial imperfection is assumed or not is the main difference between these approaches. However, the mathematical formulations of these approaches are quite analogous: if the amount of initial imperfection is set to be zero in the imperfection model, the problem is reduced to the bifurcation analysis. These approaches were reviewed and summarized by Rice [10], Needleman and Rice [11], Tvergaard [12], and Needleman and Tvergaard [13]. Within the framework of the imperfection analysis, the influence of constitutive models on the limit strains have investigated. The limit strains were found to have strong dependence on the description of the yield function, the flow rule, and the hardening rule (Bassani et al. [14], Barlat [15], Hutchinson and Neal [16], Tvergaard [17]).

Theoretical, experimental and numerical investigations on localized necking have been conducted so far by many researchers as well as engineers [18]. In the early period, investigations were directed towards the understanding of mechanisms behind localized necking. The targets of recent investigations have shifted to, in particular, the interpretation of the influence of microstructure, such as crystallographic texture, on the formability (Wu et al. [19], Yoshida et al. [3], [4]). The crystal plasticity model is adopted in the necking analysis so as to incorporate the information of crystallographic orientation. These results give guidelines for the development of high-formability sheets. Therefore, the analysis of sheet necking is still actively carried out on the basis of the crystal plasticity model. In the present paper, we demonstrate the imperfection approach of sheet necking analysis in conjunction with phenomonological and crystal plasticity models, and influences of material properties are reviewed.

Experimental results [20]-[22] and numerical results [23][24] show that the FLC depends on the strain path. The FLC corresponding to linear strain paths is therefore not a useful concept for the assessment of forming severity in forming processes with nonlinear strain paths.

Some authors have represented the forming limits using the state of stress instead of the state of strain [25]-[27]. The resulting Forming Limit Stress Curve (FLSC) is constructed by plotting the state of stress at the forming limits in stress space, and the FLSC is reported to be independent of the strain path. If path-independence of the FLSC can be established, then the limits to formability will be predicted accurately using a combination of the FLSC and finite element simulation, not only for proportional loading but also for cases with complex strain history.

Despite the usefulness of the FLSC concept awareness of the path-independence of the FLSC is not widespread. One reason is that there has been no experimental validation for the FLSC concept, because it is generally difficult to determine the exact stress state in sheet specimens experimentally except for some simple deformation mode. In the above mentioned previous studies, the authors calculated the forming limit stresses from the measured forming limit strains using a postulated yield function and isotropic hardening rule. The FLSCs thereby obtained in early work are

questionable. In these experiments a specimen undergoes two-stage strain paths and in such experiments the stress generated in the sheet metal cannot simply be predicted by the isotropic hardening assumption. Moreover, experimental verification of the constitutive model used to calculate the forming limit stresses was not carried out in these studies; usually we do not know an appropriate constitutive model for any given material and strain paths. For this reason it is vital to use an experimental method which enables an accurate measurement of stress values, in order to establish the FLSC concept.

Under these circumstances, the authors started series of works on the path-dependence of FLSC from the standpoint of both experiment and numerical computation. Firstly, Yoshida et al. [28] measured the forming limit strains and stresses of an A5154-H112 tube for linear and various combined stress paths, using a servo-controlled, internal pressure-axial load testing machine built by Kuwabara and coworkers [29][30]. Unlike in the previous studies, the forming limit stresses were determined from the load, internal pressure and geometry measurements of the tube without any assumption of the constitutive equations. They showed that the forming limit stresses fall on a single curve in stress space irrespective of the strain path. The path-independence of the FLSC was validated at least for their experimental parameters. They [28][30] also measured the plastic deformation behavior of the aluminum alloy tube, and represented the work-hardening behavior by the equivalent stress-equivalent plastic strain curve. It was found that all equivalent stress-equivalent plastic strain curves for the linear and combined stress paths almost lie on a single curve. This observation implies that the stress-strain curve of the aluminum alloy tube, not only for the linear stress path but also for the combined stress path, is well predicted by the isotropic hardening rule. In numerical studies, Yoshida et al. [1] analyzed the forming limit stresses for many two-stage combined stress paths by using the M-K model and a phenomenological plasticity theory with the isotropic hardening rule. It has been revealed that the FLSC is almost path-independent for two-stage combined stress paths which include unloading between first and second loadings. It is explained that the path-independence of the FLSC is attributed to the isotropic hardening rule used in the constitutive model. These experimental and numerical studies have demonstrated that the FLSC is path-independent when the work-hardening behavior is well described by the isotropic hardening rule. However, it is well recognized that the work-hardening behavior of steels can not be represented by the isotropic hardening rule. Yoshida et al. [31] extended their experimental work by measuring the forming limit stresses of a steel tube under linear and combined stress paths. It is showed that the forming limit stresses are path-independent when the equivalent stress-equivalent plastic strain curve for given linear and combined stress paths correspond to each other, whereas they decrease when prestraining reduces the subsequent work-hardening rate. It is concluded that the subsequent work-hardening behavior of the material plays an important role in whether the FLSC is path-independent. Yoshida and Suzuki [2] systematically investigated the influence of work-hardening behavior on the path-dependence of forming limit stresses by analyzing the forming limits for combined stress paths using the M-K model in conjunction with three types of work-hardening behavior, represented by a phenomenological work-hardening model proposed by Teodosiu and Hu [32][33]. The computational results which are consistent with their experimental observations are shown.

In the present paper, we review the experimental appratus that enables the direct measurement of stress applied to tubular or sheet specimens and demoenstrate the experimental validation of the path-independency of FLSC.

Theoretical framework

Phenomenological plasticity model. The constitutive models adopted here are the same as those used in the previous work [1], except for the associated flow rule. Rate-dependent viscoplastic material is concerned. The dynamic yield surface is assumed to be given by

$$f = J(\boldsymbol{\sigma}, \mathbf{n}_i, \bar{\varepsilon}) - g(\bar{\varepsilon})\left(\frac{\dot{\Phi}}{\dot{\Phi}_0}\right)^m = 0\,, \tag{1}$$

where J is an equivalent stress which is a function of the Cauchy stress $\boldsymbol{\sigma}$, $\mathbf{n}_i$ are the orthotoropic anxes, $\bar{\varepsilon}$ is an equivalent strain, g is a strain hardening function, $\dot{\Phi}_0$ is a reference value of the overstress function, and m is a rate sensitivity parameter.
In this analysis we use the associated flow rule, hence the direction of plastic strain rate is identical to the direction normal to the yield surface.

$$\mathbf{D}^{\mathrm{p}} = \dot{\Phi}\mathbf{N}\,, \quad \mathbf{N} \equiv \frac{\partial J / \partial \boldsymbol{\sigma}}{\| \partial J / \partial \boldsymbol{\sigma} \|}, \tag{2}$$

where is the unit tensors normal to the dynamic yield surface. We use the function proposed by Barlat and Lian [34] to define J in Eq. 1,

$$J(\boldsymbol{\sigma}, \mathbf{n}_i, \bar{\varepsilon}) \equiv \left[\frac{1}{2}\left\{\hat{a}\left|K_1 + K_2\right|^M + \hat{a}\left|K_1 - K_2\right|^M + (2-\hat{a})\left|2K_2\right|^M\right\}\right]^{1/M}, \tag{3}$$

$$K_1 = \frac{\hat{\sigma}_{11} + \hat{h}\hat{\sigma}_{22}}{2}\,, \quad K_2 = \sqrt{\left(\frac{\hat{\sigma}_{11} - \hat{h}\hat{\sigma}_{22}}{2}\right)^2 + \hat{p}^2\hat{\sigma}_{12}{}^2}\,, \tag{4}$$

where $\hat{\sigma}_{ij}(= \mathbf{n}_i \cdot \boldsymbol{\sigma} \cdot \mathbf{n}_j)$ are components of the Cauchy stress tensor with reference to the orthotropic axes, and $\hat{a}$, $\hat{h}$, $\hat{p}$ are anisotropic parameters. The parameter M governs the cavature of the yield suraface. Eq. 3 reduces to Hill's quadratic yield function for the case of $M = 2$ and corresponds to von Mises yield function if $M = 2$ and $\hat{a} = \hat{h} = \hat{p} = 1$. It is known that the yield surfaces for $M = 6$ and 8 are in good agreement with those for bcc and fcc polycrystalline sheets [35]. Anisotropic parameters are commonly identified using *r*-value, which is the ratio of width strain to thickness strain under uniaxial tension. We employ the following power law function as a hardening rule,

$$g(\bar{\varepsilon}) = k(\varepsilon_0 + \bar{\varepsilon})^n\,, \tag{5}$$

where k, ε_0, n are the material parameters.

Crystal plasticity model. The crystal plasticity model formulated by Peirce et al. [36] and Asaro and Needleman [37] is used here. The velocity gradient $\mathbf{L}$ is decomposed into the elastic contributing part $\mathbf{L}^*$ and the plastic part $\mathbf{L}^{\mathrm{p}}$. Plastic deformation is considered to arise from slip on slip systems:

$$\mathbf{L}^{\mathrm{p}} = \mathbf{D}^{\mathrm{p}} + \mathbf{W}^{\mathrm{p}} = \sum_\alpha \dot{\gamma}^{(\alpha)}\mathbf{p}^{(\alpha)} + \sum_\alpha \dot{\gamma}^{(\alpha)}\mathbf{w}^{(\alpha)}\,, \tag{6}$$

$$\mathbf{p}^{(\alpha)} = \frac{1}{2}(\mathbf{s}^{(\alpha)} \otimes \mathbf{m}^{(\alpha)} + \mathbf{m}^{(\alpha)} \otimes \mathbf{s}^{(\alpha)})\,, \quad \mathbf{w}^{(\alpha)} = \frac{1}{2}(\mathbf{s}^{(\alpha)} \otimes \mathbf{m}^{(\alpha)} - \mathbf{m}^{(\alpha)} \otimes \mathbf{s}^{(\alpha)})\,, \tag{7}$$

where the plastic part of rate of deformation $\mathbf{D}^{\mathrm{p}}$ and the plastic spin $\mathbf{W}^{\mathrm{p}}$ are, respectively, the symmetric and antisymmetric parts of $\mathbf{L}^{\mathrm{p}}$, $\dot{\gamma}^{(\alpha)}$ is the slip rate, and $\mathbf{s}^{(\alpha)}$ and $\mathbf{m}^{(\alpha)}$ are, respectively, the slip direction and slip plane normal for the α th slip system. In the present work, the face-centered-cubic crystal structure with 12 slip systems of $\{111\}\langle 110\rangle$ is considered.
The slip rate $\dot{\gamma}^{(\alpha)}$ is assumed to be given by a power law dependence on the resolved shear stress $\tau^{(\alpha)}$ on the α th slip system,

$$\dot{\gamma}^{(\alpha)} = \dot{\gamma}_0 \operatorname{sgn}(\tau^{(\alpha)}) \left| \frac{\tau^{(\alpha)}}{g^{(\alpha)}} \right|^{1/m}, \tag{8}$$

where $\dot{\gamma}_0$ is the reference slip rate, m is the strain-rate sensitivity exponent, and $g^{(\alpha)}$ is the slip resistance. The evolution law for $g^{(\alpha)}$ is specified by

$$\dot{g}^{(\alpha)} = h \sum_{\beta} |\dot{\gamma}^{(\beta)}|, \quad h = h_0 \left(1 + \frac{h_0 \gamma_{\mathrm{a}}}{\tau_0 n} \right)^{n-1}, \quad \gamma_{\mathrm{a}} = \int_0^t \sum_{\alpha} |\dot{\gamma}^{(\alpha)}| \, \mathrm{d}t, \tag{9}$$

where τ_0 is the initial value of $g^{(\alpha)}$, h_0 is the initial slip hardening modulus, n is the power-law hardening exponent, and t is time.
A generalized Taylor-type model is adopted, namely, the velocity gradient in each grain is taken to be identical to the macroscopic velocity gradient. Taking the volume fraction of each grain to be identical, the macroscopic stress $\bar{\boldsymbol{\sigma}}$ and macroscopic plastic part of the rate of deformation $\bar{\mathbf{D}}^{\mathrm{p}}$ are obtained by averaging the values over the total number of grains.

Problem formulation

Occurrence of localized necking is analyzed using an imperfection model proposed by Marciniak and Kuczyński [8]. A band-type thickness imperfection is assumed (Fig. 1). In the undeformed state the orthonormal axes $\hat{x}_i$ are taken to coincide with the fixed Cartesian axes x_i. The quantities inside the band are denoted by $(\,)^{\mathrm{b}}$. The initial thickness inside and outside the band are respectively denoted by h_0^{b} and h_0. The initial geometric non-uniformity is specified by $f_0 = h_0^{\mathrm{b}} / h_0$. The current unit normal of the band is $\bar{\mathbf{m}} = (\cos\psi, \sin\psi)$, where ψ is the angle between $\bar{\mathbf{m}}$ and x_1. Since uniform deformation fields are assumed both inside and outside the band, equilibrium and compatibility inside these two regions are automatically satisfied, apart from the necessary conditions along the edge of the band. For the thin sheets considered here, in-plane stretching results in a plane stress state. Thus, the components L_{13}, L_{31}, L_{23} and L_{32} are automatically zero. The compatibility at the band interface is given in terms of the differences in the velocity gradients inside and outside the band,

$$L_{ij}^{\mathrm{b}} = L_{ij} + \dot{c}_i \bar{m}_j, \tag{10}$$

where subscripts are 1 or 2, and $\dot{c}_1$ and $\dot{c}_2$ are the parameters to be determined. Using current values of the thickness inside and outside the band (h^{b}, h), the equilibrium condition at the band interface is given by

$$\bar{m}_i \sigma_{ij}^{\mathrm{b}} h^{\mathrm{b}} = \bar{m}_i \sigma_{ij} h. \tag{11}$$

For deformation outside the band we set $L_{12} = L_{21} = D_{12} = W_{21} = 0$. The in-plane normal components of the velocity gradient $L_{11}(= D_{11})$ and $L_{22}(= D_{22})$ are specified. Here, linear strain path is applied to the material element by holding the ratio $\rho = L_{22} / L_{11}$ constant.

By substituting the constitutive relation in plane stress form into the rate form of Eq. 13, and eliminating L_{ij}^{b} using Eq. 10, we obtain simple algebraic equations having two unknowns, $\dot{c}_1$ and $\dot{c}_2$. From the solutions we can calculate all of the rate values of the variables to be updated.

The onset of localized necking is defined by the occurrence of a much higher maximum principal strain rate inside the band than outside the band, $\dot{\varepsilon}_1^{\mathrm{b}} / \dot{\varepsilon}_1 \geq 10^5$, where $\dot{\varepsilon}_1$ and $\dot{\varepsilon}_1^{\mathrm{b}}$ respectively denote the maximum principal values of the rate-of-deformation tensors **D** and $\mathbf{D}^{\mathrm{b}}$. Limit strains are computed for varying an initial band angle ψ_0, and the miniumum is defined as the forming limit strain. If f_0 is taken to be unity, trivial solutions of $\dot{c}_i$ are always zero and nontrivial solutions exist at the bifurcation point. The bifurcation analysis can also be performed based on this problem formulations [5], [11], [13].

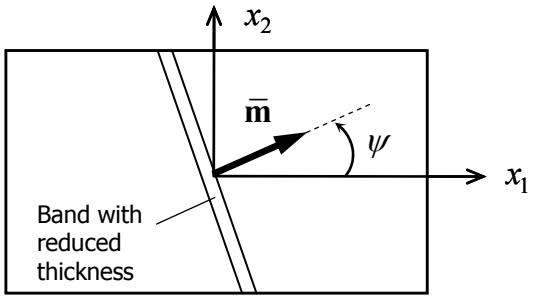

Fig. 1. A thin sheet with an initial thickness imperfection

Results of analysis of forming limit curves

Phenomenological plasticity model. The material parameters and initial thickness imperfection used in the present computation are as follows: $M = 8$, $n = 0.35$, $k = 490$MPa, $\varepsilon_0 = 0.00285$, $m = 0.002$, $\bar{r} = 1$, and $f_0 = 0.999$. For the simplicity, let us neglect in-plane anisotropy, namely the *r*-value for any direction in the sheet plane is identical and is denoted by $\bar{r}$. Fig. 2 shows the influence of material parameters and initial imperfection on predicted forming limit curve (FLC). In Fig. 2(a), we have examined the impact of the yield surface curvature by varying M. When $M = 2$, the yield surface corresponds to von Mises yield surface. Left side of FLC is almost insensitive to M, whereas the right hand side of FLC, in particular, around equi-biaxial stretching mode have strong dependence on M. In Fig. 2(b), the effects of n and $\bar{r}$ are investigated by keeping the other parameters unchanged. The limit strains increase as n increases over the whole range of FLC. The limit strains for $\bar{r} = 0.5$, 1, and 2 falls on the same line. Thus, the anisotropy of material has no influence on limit strains, however it is limited to the case in which the in-plan isotropy is assumed and Eq. 3 is employed in the constitutive model. In Fig. 2(c), influences of strain rate sensitivity and magnitude of initial imperfection are shown. Limit strains are enhanced as m increases. This effect is greater for the left side of FLC than the right side of it. On the other hand, the influence of initial imperfection parameter is more significant in the right hand side of FLC. The effects of material parameters have been demonstrated and more details were reported in the literatures: effects of yield surface in [38]-[42], strain rate sensitivity in [43], [44], strain path change in [24], [45].

Crystal plasticity model. Forming limits of textured fcc polycrystalline sheets are investigated in the previous work [3], and the main conclusions are presented here briefly. Five textured sheets which are typically observed in aluminum alloy sheet are generated in computer. As the rolled texture, copper, S, and brass textures are considered, and the cube and Goss textures are generated as the recrystallization texture. The influence of the texture components on the limit strain is numerically investigated using crystal plasticity model in conjunction of the M-K type model. In addition to the five texture components, random texture is considered as the reference. Fig. 2(d) shows FLCs for the textured sheets. The influence of texture is dramatic on the right hand side of FLC. Only cube texture yield FLC higher than the random texture, and all the other texture

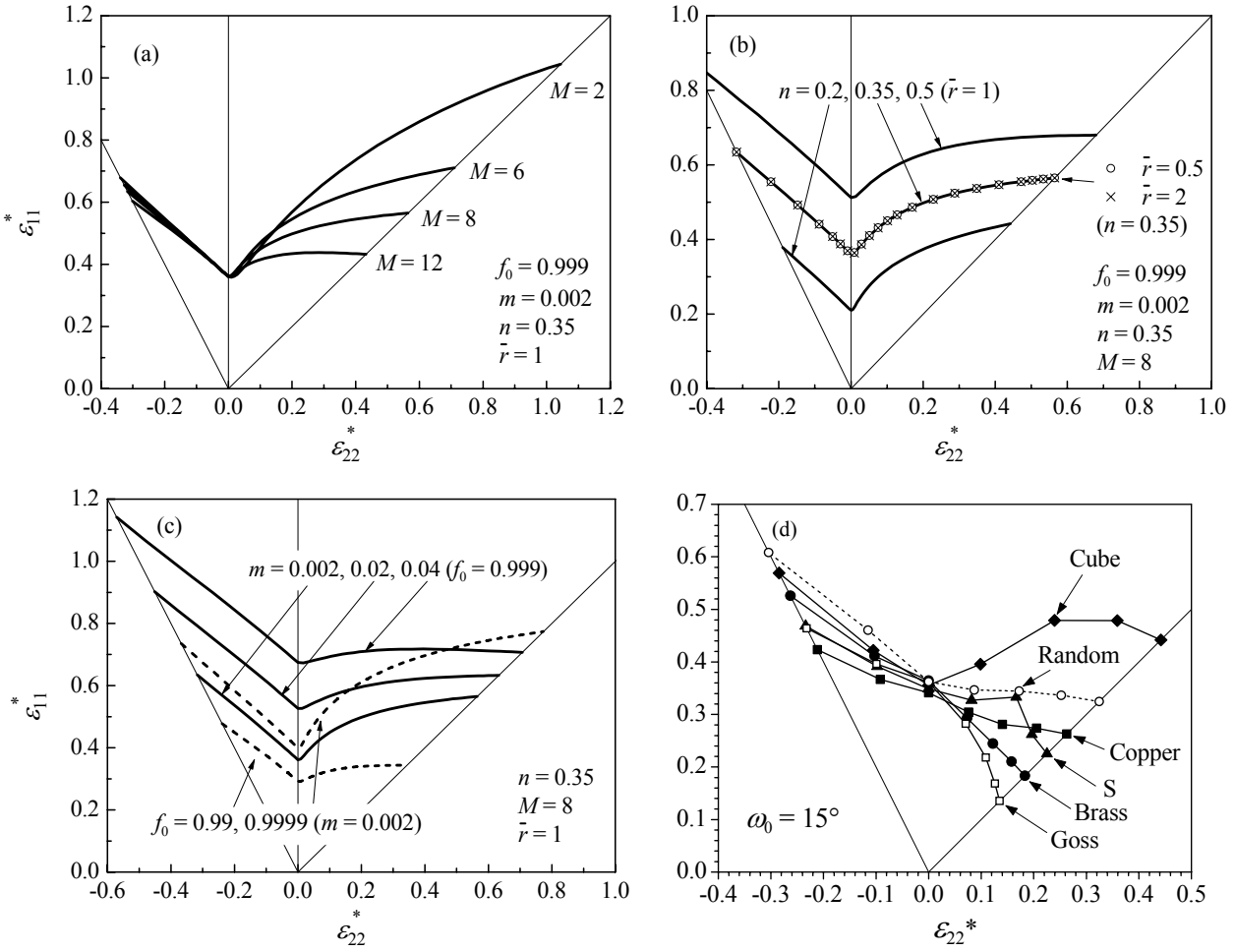

Fig. 2. Influence of yield surface curvature (a), anisotropy and work-hardening exponent (b), and strain-rate sensitivity and initial thickness imperfection on predicted forming limit curves. Forming limit curve simulated for textured aluminum sheet (d).

components yields lower limit strains. It is, therefore, concluded that the reduction of the volume fraction of these texture components and generation of cube orientation can be effective for improving the formability of aluminum alloy sheets.

Experimental methods for determining Forming Limit Curve (FLC) and Forming Limit Stress Curve (FLSC)

Punch-stretch testing method. A punch-stretch testing apparatus and specimen geomtery used to detemine foming limit strains of sheet metals are shown in Fig. 3. This testing method was first proposed by Marciniak and Kuczyński [8]. The cylindrical punch exerts a pressure on the specimen, not directly, but through a auxiliary sheet with a circular hole. Since, during punch-stretching, material elements in the auxiliary sheet move in a radial direction more rapidly than those in the specimen, the frictional, radial forces appear in the region of contact between the specimen and auxiliary sheet. This friction prevents the specimen from fracturing near the rounded edge of the punch and results in the largest strains taking place in the central part of the specimen at the flat bottom of the punch. Strain ratios exerted to the specimens can be changed by changing the width or the distance between the circular notches of the specimen. A grid of square is used in the measurement of forming limit strains. After forming, the strains to the onset of localized necking are

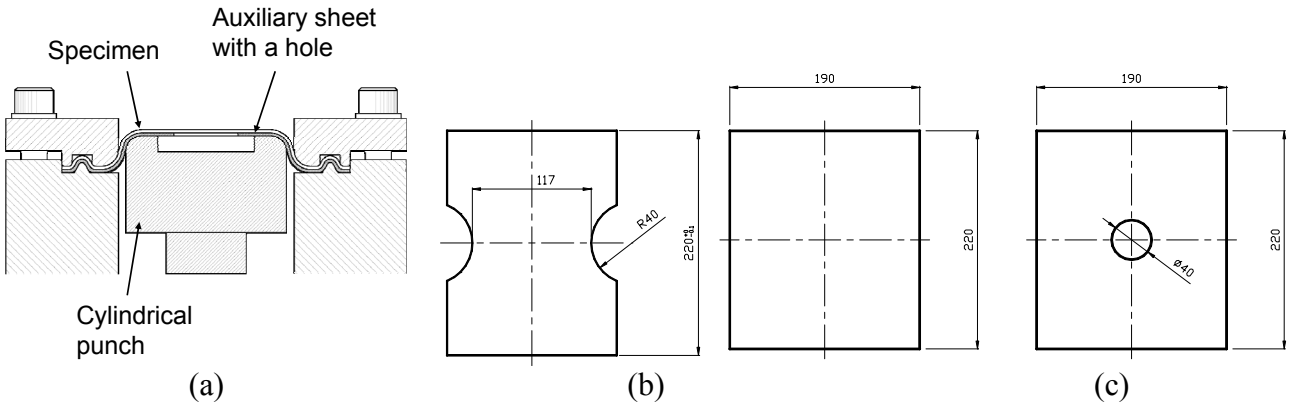

Fig. 3. Experimental method for determining forming limit strains for sheet metals (Marciniak-Kuczyński method [8]); (a) punch-stretch testing apparatus, (b) specimans with different geometries, and (c) auxiliary sheet with a circular hole.

measured from the nearest squares to the fracture.

Figure 4 shows the measured forming limit curves (FLCs) for two kinds of as-received aluminum alloy sheets (1mm thick) with different Mg contents: Al-2.5%Mg and Al-5.5%Mg [46]. Limit strains of Al-2.5% Mg are larger than those of Al-5.5% Mg in almost all biaxial tension regions, but the order of formability is reversed from the plane-strain to uniaxial tension regions, in line with earlier reports [47], [48]. The FLCs calculated using the Marciniak-Kuczyński approach [8] with the Yld2000-2d yield function [49][50], the unknown material parameters of which were determined using the biaxial tensile testing method using a cruciform specimen [51], are in fair agreement with the observed one for Al-5.5% Mg (Fig. 5(a)), whereas underestimate the observed limit strains for Al-2.5% Mg in the biaxial stretching region (Fig. 5(b)) because of unknown reason.

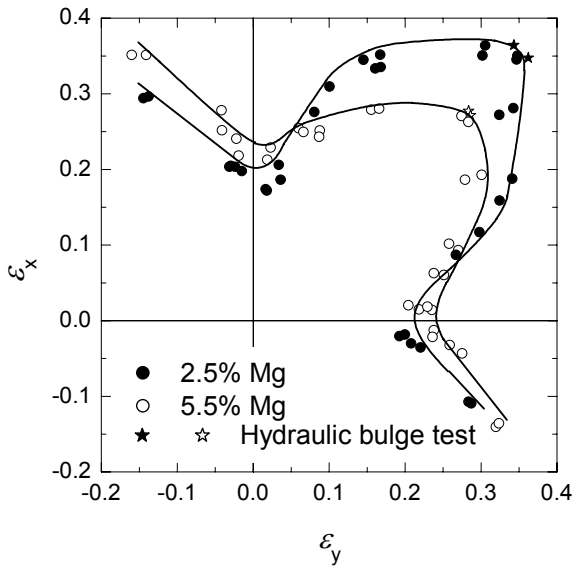

Fig. 4. Forming limit curves for two kinds of as-received aluminum alloy sheets with different Mg contents: Al-2.5%Mg and Al-5.5%Mg [46].

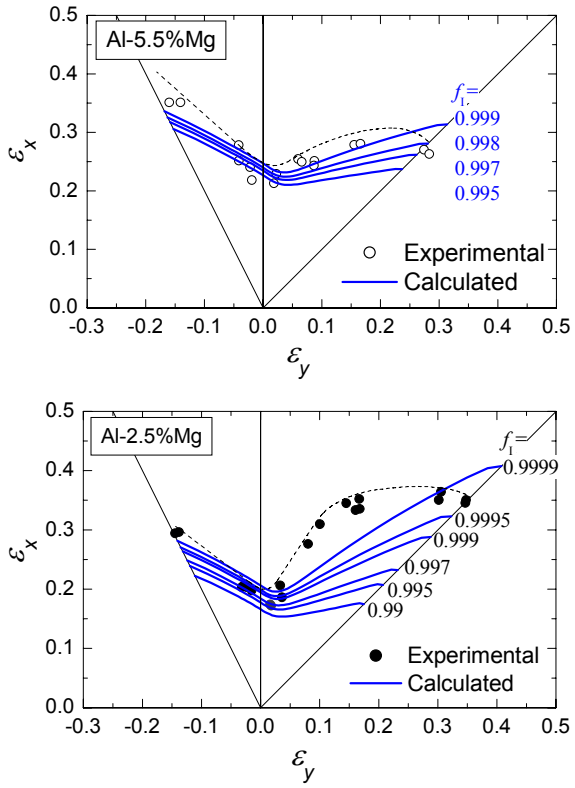

Fig. 5. Measured forming limit strains compared with calculated forming limit curves [46].

Multiaxial tube expansion testing method: tubular material. The demand for accurate prediction of forming limits of sheet metal parts with complicate geometry using a finite element analysis is increasing. Formability of sheet metals has been evaluated conventionally using the forming limit curve (FLC) in strain space determined from linear strain paths. However, the FLC cannot be used for combined (nonlinear) strain paths, because it changes, depending on strain paths [20]-[24].

On the other hand, some authors have represented the forming limit using the state of stress rather than the state of strain and the resulting *Forming Limit Stress Curve* (FLSC), constructed by plotting the state of stress at the forming limits in stress space, is reportedly independent of the strain path [25]-[27]. Yoshida and coworkers experimentally measured the forming limit stress of aluminum alloy tube [28] and steel tube [31] and concluded that the FLSC is path-independent if the material work hardens isotropically [1].

Figure 6 shows the forming limit curves of extruded aluminum alloy tube measured using a combined tension-internal pressure testing machine developed by Kuwabara et al. [29], [30]. The axial load and internal pressure were servo-controlled using an electrical, closed-loop control system, and were applied simultaneously to a tubular specimen so that arbitrary stress paths could be applied to the specimen. To determine the FLCs and FLSCs for the test material, linear and combined stress path tests were performed. In the linear stress path experiments, biaxial stresses were applied to the

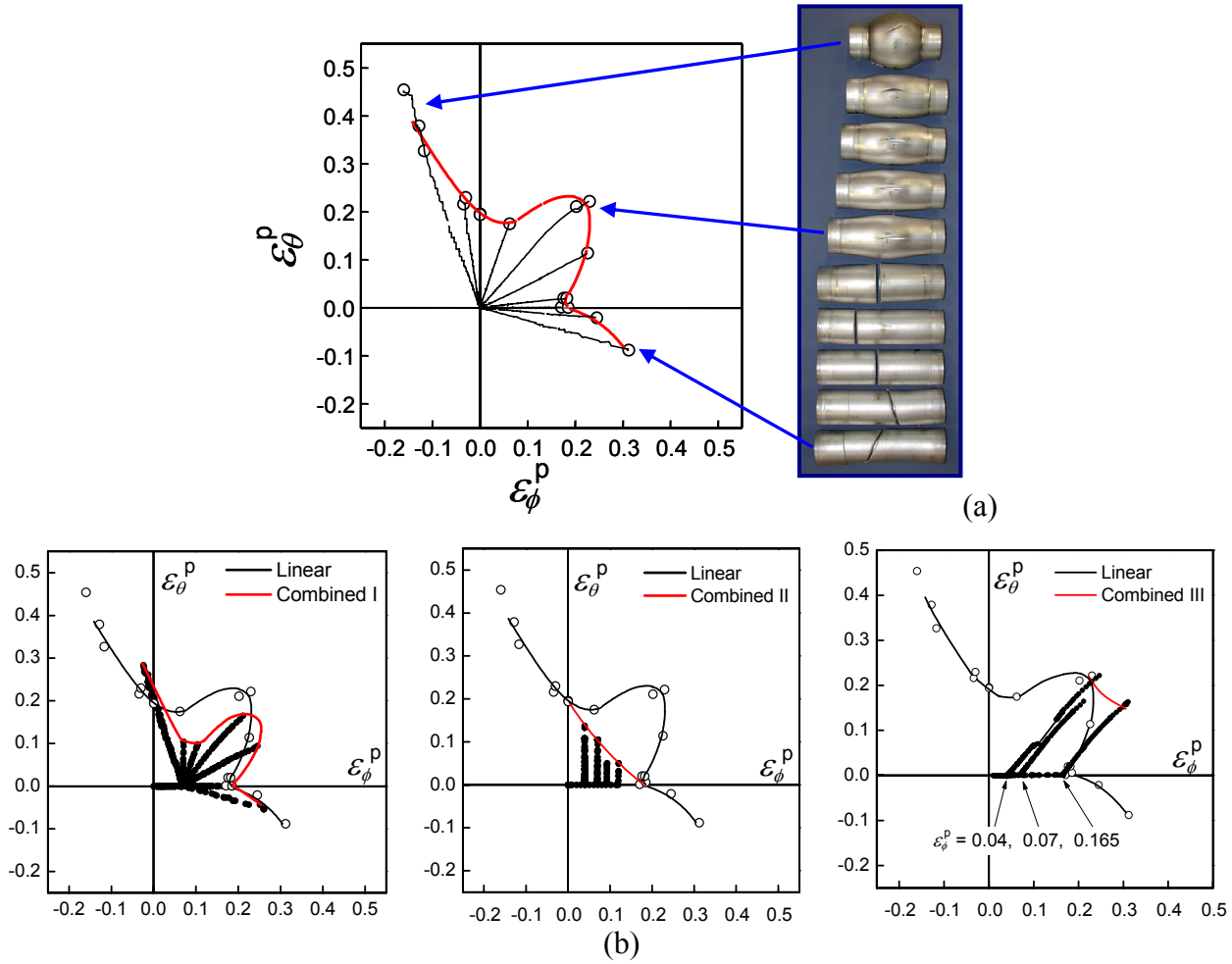

Fig. 6 Multiaxial tube expansion test of an extruded aluminum alloy tube, JIS A5154-H112, of outer diameter 76.3mm and wall thickness 3.9mm [28]. Forming limit curves for (a) linear and (b) combined stress paths I, II and III.

specimens with the stress ratios in certain proportions, namely $\sigma_\phi : \sigma_\theta$ (axial true stress) : (circumferential true stress) =1:0, 4:1, 2:1, 4:3, 1:1, 20:23, 3:4, 1:2, 1:4 and 0:1, until the specimens burst. Here, $\sigma_\phi : \sigma_\theta =$ 20:23 is the stress ratio for which the ratio of the plastic strain increments, $\mathrm{d}\varepsilon_\theta^{\mathrm{p}}/\mathrm{d}\varepsilon_\phi^{\mathrm{p}}$, is close to unity. In addition, three types of combined stress path experiments were carried out as follows:

Combined stress path I: Specimens were loaded at $\sigma_\phi : \sigma_\theta = 2{:}1$ (near plane strain tension in the axial direction) until $\varepsilon_\phi^{\mathrm{p}}$ reached 0.07. After unloading, the specimens were reloaded at $\sigma_\phi : \sigma_\theta =$ 1:0, 2:1, 1:1, 20:23, 3:4, 1:2 and 0:1, until they burst.

Combined stress path II: Specimens were loaded at $\sigma_\phi : \sigma_\theta = 2{:}1$ until $\varepsilon_\phi^{\mathrm{p}}$ reached 0.04, 0.07, 0.093 and 0.12. After unloading, the specimens were reloaded at $\sigma_\phi : \sigma_\theta = 1{:}2$ until they burst.

Combined stress path III: Specimens were loaded at $\sigma_\phi : \sigma_\theta = 2{:}1$ until $\varepsilon_\phi^{\mathrm{p}}$ reached 0.04, 0.07 and 0.165. After unloading, the specimens were reloaded at $\sigma_\phi : \sigma_\theta = 20{:}23$ until they burst.

Figure 6 shows that the FLCs strongly depend on the strain history, in line with earlier studies [20]-[24].

The forming limit stresses measured for linear and combined stress paths I, II, and III are shown in Fig. 7. The open circles, ○, indicate the forming limit stresses measured for the linear stress paths, and the solid line fitted to the forming limit stresses is the FLSC for the linear stress paths. The FLSC is concave at stress ratios $\sigma_\phi : \sigma_\theta = 1{:}2$ and 2:1 (near plane-strain tension), and is very sharp in the direction of the stress ratio $\sigma_\phi : \sigma_\theta = 20{:}23$. The forming limit stresses observed for the combined stress paths I, II, and III lie close to a single curve. We therefore conclude that the FLSC is independent of the stress path, at least for the present experimental parameters. Moreover, we conclude that the forming limit stresses are almost independent of the amount of prestrain, since the forming limit stresses observed for the combined stress paths II or III fall almost at a single point.

Yoshida et al. [1] discussed the strain-path dependence of the forming limit stress by observing the strain localization process using the Marciniak and Kuczyński model and a phenomenological plasticity model with non-normality effects [52]. It is found that forming limit stress is almost path-independent provided that the work-hardening behavior is not affected by the strain-path change. Thus, for a material exhibiting such behavior, the FLSC method is worthwhile for assessment of forming

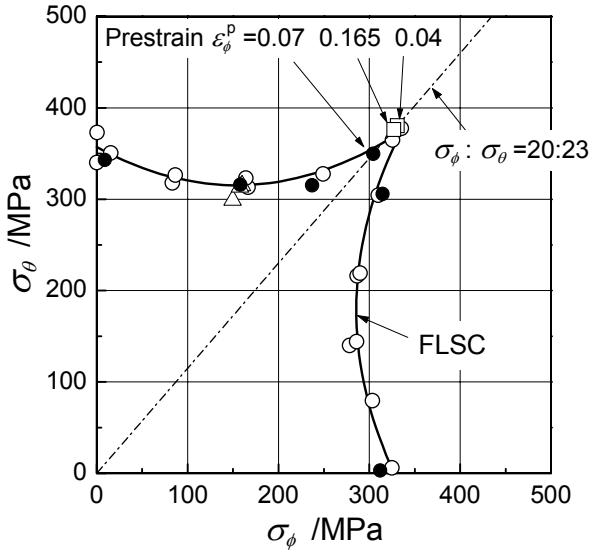

Fig. 7. Forming limit stresses for linear (○) and combined stress paths I (●), II (△) and III (□) [28].

severity. When the work-hardening after prestrain is affected by strain-path change, as is observed for steel tube [31], the FLSC is no longer path-independent. Thus, the work-hardening behavior of a material plays an important role and should be checked before adopting the FLSC method.

Multiaxial tube expansion testing method: sheet material. Ishiki et al. [53] investigated the work hardening of pure titanium sheet under biaxial tension for a strain range up to 0.085. Pure titanium sheet was manually bent and welded to fabricate tubular specimens and to perform biaxial tensile tests for many linear stress paths using the closed-loop electrically servo-controlled tension-internal pressure testing apparatus developed in [29], [30]. This experimental technique is extremely effective to measure the biaxial stress-strain curves of sheet metals under arbitrary stress paths for a large strain range up to fracture, because, in the biaxial tensile test with a cruciform specimen fracture occurs at an early stage of plastic deformation in one of the arms; the maximum plastic strain applicable to pure titanium sheet is approximately 0.001. On the other hand, one of the shortcomings of this testing method is that strain gauges have to be changed every strain increment of 0.1.

The authors' research group has developed a new multiaxial tube expansion testing machine, in which a new strain measurement system that enables continuous measurement of biaxial stress-strain curves, from initial yielding up to fracture, is installed [54].

Figure 8 shows the biaxial stress-strain curves of the cold rolled, interstitial free (IF) steel sheet measured using the multiaxial tube expansion testing machine for linear stress paths. The dotted lines in each figure are those measured using the biaxial tensile tests using cruciform specimens as proposed in [51]. The former smoothly connects to the latter by offsetting the former along the strain axis by an appropriate amount of strain increment. This offsetting procedure is necessary to appropriately reflect the amount of work hardening applied to the sheet sample during tube fabrication in the stress-strain curves measured for the tubular specimens.

The concept of the contour of plastic work in the stress space [55], [56] was used to evaluate the

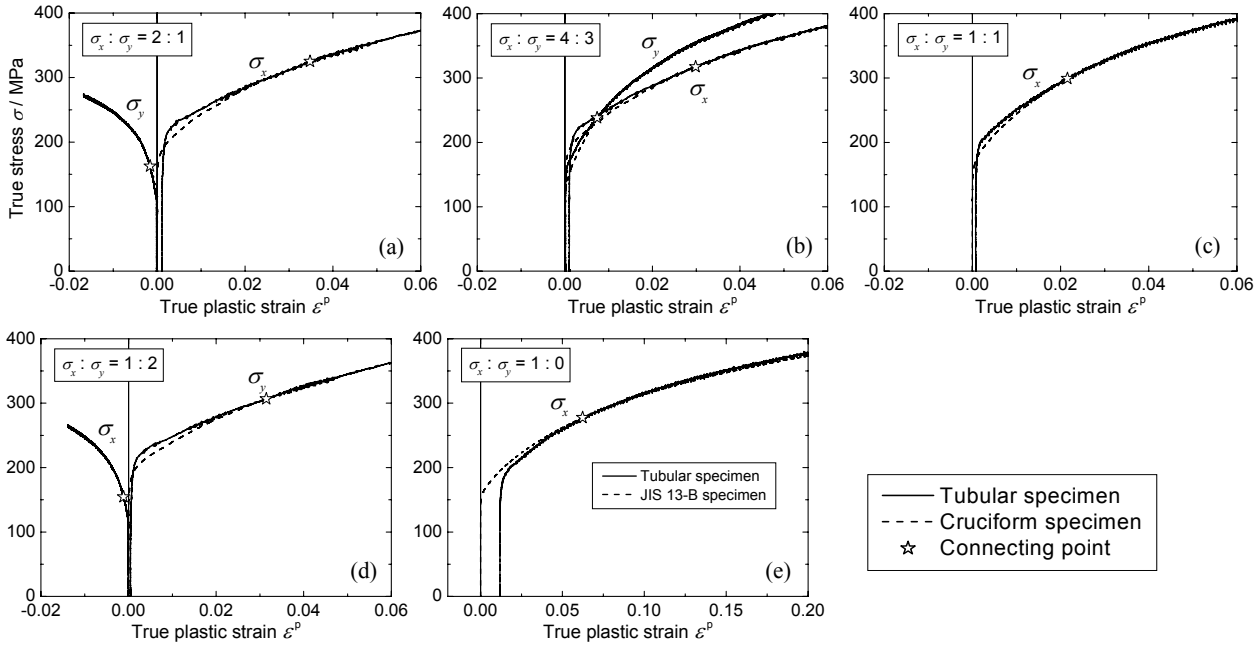

Fig. 8. Measured biaxial stress-strain curve (solid lines) of IF steel sheet for $\sigma_x : \sigma_y$ (σ_x: true stress in rolling direction and σ_y: true stress in transverse direction) =(a) 2:1, (b) 4:3, (c) 1:1, (d) 1:2 and (e) 1:0 measured using a multiaxial tube expansion testing machine. The dashed lines are those measured using the cruciform specimen, as proposed in [51], which smoothly connect to the former at the star marks, ☆.

work hardening behavior of the test material under biaxial tension. The stress-strain curve obtained from a uniaxial tensile test along the RD of the material was selected as a reference datum for work hardening; the uniaxial true stress σ_0 and the plastic work per unit volume W_0 corresponding to particular values of offset logarithmic plastic strains $\varepsilon_0^{\mathrm{p}}$ were determined. The uniaxial true stress σ_{90} obtained from a uniaxial tensile test along the TD and the biaxial true stress components (σ_x, σ_y) obtained from biaxial tensile tests were then determined at the same plastic work as W_0. The stress points $(\sigma_0, 0)$, $(0, \sigma_{90})$ and (σ_x, σ_y) plotted in the principal stress space comprise a contour of plastic work corresponding to a particular value of $\varepsilon_0^{\mathrm{p}}$. For a sufficiently small value of $\varepsilon_0^{\mathrm{p}}$ the corresponding work contour can be practically viewed as a yield locus.

Figure 9 (a) shows the measured stress points that comprise the contours of plastic work for different levels of $\varepsilon_0^{\mathrm{p}}$. The experimental scatter was less than 1% of the flow stress. The work contours were successfully measured up to $\varepsilon_0^{\mathrm{p}} = 0.15$. In Fig. 9(b) the stress values corresponding to a specific value of $\varepsilon_0^{\mathrm{p}}$ are normalized by the σ_0 belonging to the same group of work contour to observe a variation of work contour shape with $\varepsilon_0^{\mathrm{p}}$, It is found that the test material exhibits differential work hardening; the shapes of work contours change with $\varepsilon_0^{\mathrm{p}}$. Also depicted in Fig. 9(b) are the yield loci based on the von Mises, Hill's quadratic and the Yld2000-2d yield functions with exponents of $M = 4$ and 6 [49]. Standard deviation of the theoretical yield loci from the measured work contours was calculated to quantitatively evaluate the most suitable yield function for the sample. It was found in Fig. 9(b) that the Yld2000-2d with $M = 6$ has closer agreement with the experimental data at a strain level of $\varepsilon_0^{\mathrm{p}} = 0.15$.

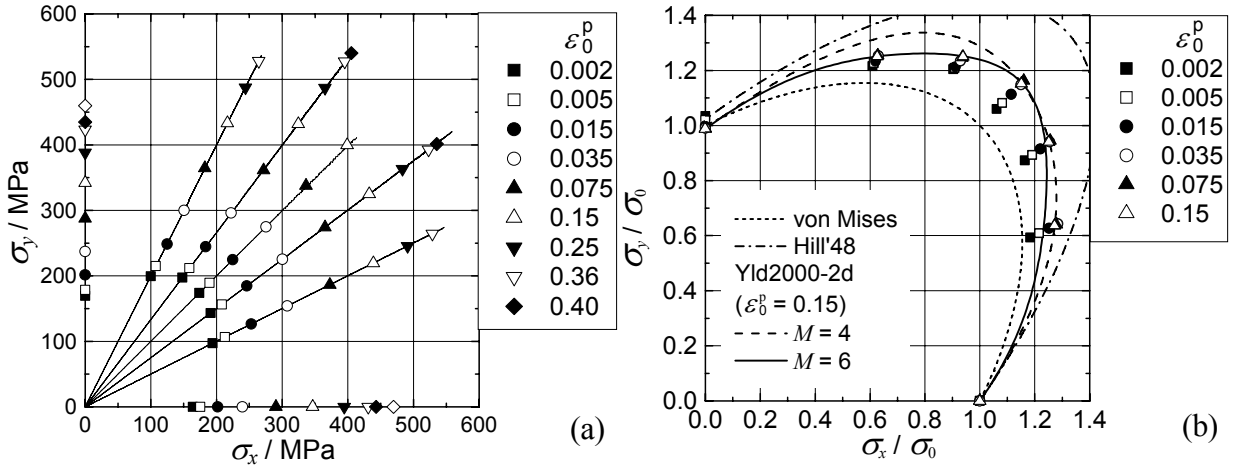

Fig. 9 Measured stress points comprising contours of plastic work.

Figure 10 (a) and (b) shows the forming limit strains and forming limit stresses of the test material, respectively. The marks □ and ★ indicate that fracture occurred at a position of $\theta \le \pm 30°$ and $\theta > \pm 30°$, respectively, where θ is the angle from the weld line in the circumferential direction of the tubular specimen. Therefore, ★ is deemed to represent the real forming limit strains and stresses of the test material as the position of fracture is far enough from the weld line. It is also noted that □ is very close to ★; the difference in the amount of strain between □ and ★ for $\sigma_x : \sigma_y = 2{:}1$ and 4:3 is 0.01 and 0.02, respectively. The differences are almost within the error of strain measurement. Therefore, □ is also deemed to represent the real forming limit strain and stress of the test material.

Figure 10 (c) shows fractured specimens. Localized necking appeared all around the bulged area of the specimen for all stress ratios except for $\sigma_x : \sigma_y = 1{:}1$.

We could not measure the forming limit strains for $\sigma_x : \sigma_y = 1{:}1$, 1:0 and 0:1, because the specimens fractured in the weld line for $\sigma_x : \sigma_y = 1{:}1$ and buckled near the chucks for $\sigma_x : \sigma_y = 1{:}0$ and 0:1. Therefore, hydraulic bulge test and uniaxial tensile test were performed to measure the forming limit strains and stresses for $\sigma_x : \sigma_y = 1{:}1$, 1:0 and 0:1. The measured results are included in Fig. 10(a) and (b). Using the multiaxial tube expansion test, hydraulic bulge test and uniaxial tensile test, the forming limit strains and stresses under linear stress paths could be fully determined in the first quadrant of stress space.

Figure 10(a) and (b) includes the calculated FLC and FLSC based on the Marciniak-Kuczyński approach [8] using the Yld2000-2d yield function with an exponent of 6 as determined in Fig. 9(b). The magnitude of initial imperfection was chosen to be 0.994 and the strain rate sensitivity exponent (*m*-value) 0.02. The calculated FLC and FLSC are in fair agreement with the experimental data, validating the Marciniak-Kuczyński approach.

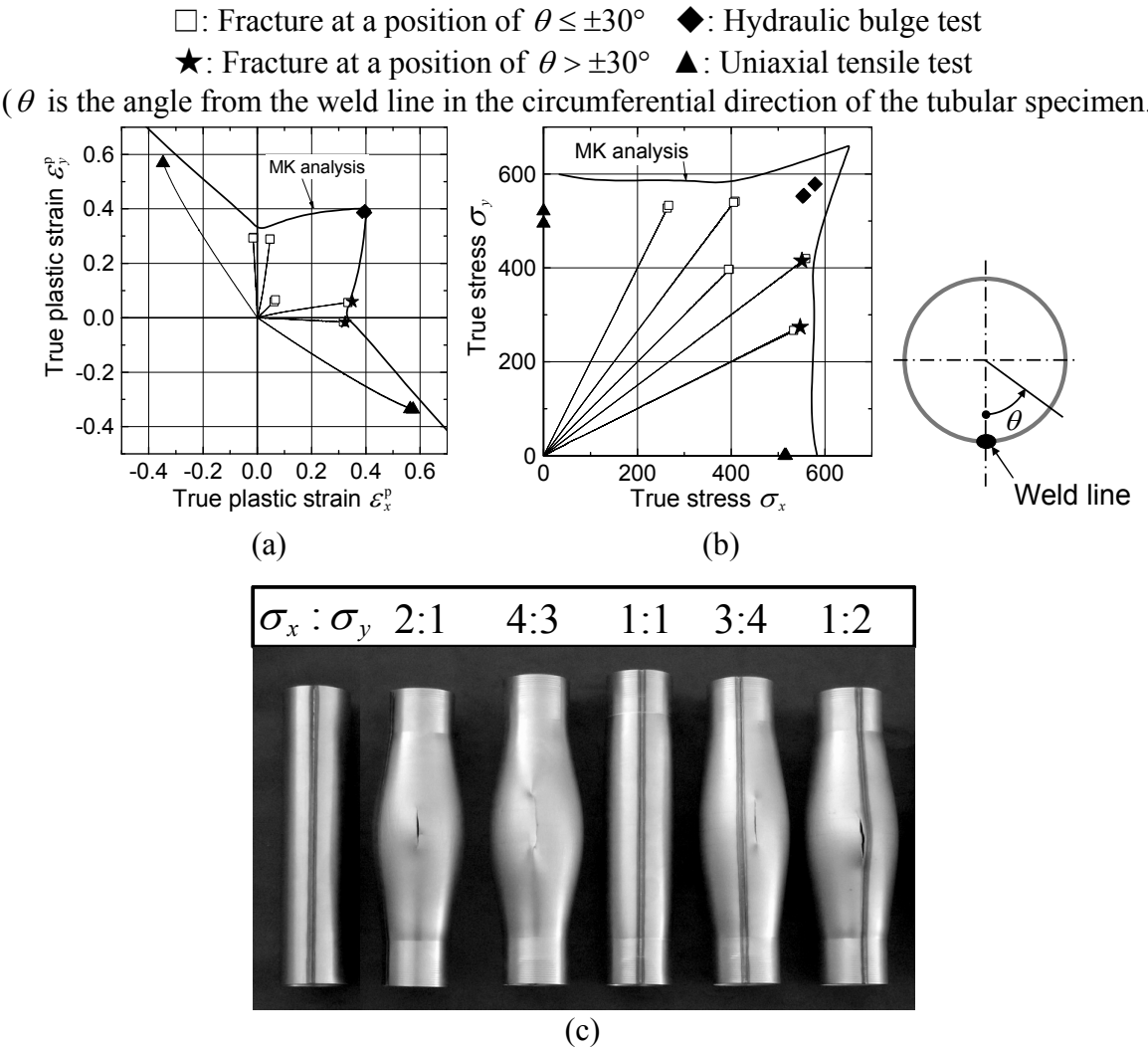

Fig. 10. Experimental results of the multiaxial tube expansion tests for interstitial free (IF) steel sheet; (a) Forming limit strains, (b) forming limit stresses and (c) fractured specimens obtained for linear stress paths.

Conclusions

In the present paper, we have demonstrated the imperfection approach of sheet necking analysis, and the influence of the various material parameters on the onset of strain localization has been shown. In the framework of the phenomenological plasticity model, yield surface curvature and the magnitude of thickness imperfection affects, in particular, the right side of FLC. On the other hand, the strain-rate sensitivity has much impact on the left side of it than the right side. From the analysis based on the crystal plasticity model, the significance of initial texture of polycrystalline sheet has been shown. The cube texture has been found to possess the potential to increase the formability in biaxial stretching mode. This type of simulation would contribute to the optimization of texture component and to the elaboration of novel high-formability sheet.

In the series of experimental works the FLC and FLSC for aluminum alloy tube [28], steel tube [31] and steel sheet [54] have been accurately measured using the tension-internal pressure type testing machine, and the measured results have been compared with those computed using the Marciniak-Kuczyński approach. From these experimental and numerical investigations the following conclusions have been obtained. Forming limit stress is almost path-independent provided that the work-hardening behavior is not affected by the strain-path change. Thus, for a material exhibiting such behavior, the FLSC method is worthwhile for assessment of forming severity. When the work-hardening after prestrain is affected by strain-path change, the FLSC is no longer path-independent. Thus, the work-hardening behavior of a material plays an important role and should be checked before adopting the FLSC method for forming limit prediction.

References

[1] K. Yoshida, T. Kuwabara, M. Kuroda, Int. J. Plasticity, 23 (2007), 361-384.
[2] K. Yoshida, N. Suzuki, Int. J. Plasticity, 24 (2008), 118-139.
[3] K. Yoshida, T. Ishizaka, M. Kuroda, S. Ikawa, Acta Mater. 55 (2007), 4499-4506.
[4] K. Yoshida, Y. Tadano, M. Kuroda, Comp. Mater. Sci. 46 (2009), 459-468.
[5] K. Yoshida, M. Kuroda, Int. J. Solids Struct. accepted.
[6] T. Kuwabara, Int. J. Plasticity 23 (2007), 385-419.
[7] R. Hill, J. Mech. Phys. Solids 1 (1952), 19-30.
[8] Z. Marciniak, K. Kuczyński, Int. J. Mech. Sci. 9 (1967), 609-620.
[9] S. Stören, J.R. Rice, J. Mech. Phys. Solids 23 (1975), 421-441.
[10] J.R. Rice, In Proc. IUTAM Congress, Theoretical and Applied Mechanics, (ed. Koiter W. T.), (1976), pp. 207-220.
[11] A. Needleman, J.R. Rice, In Mechanics of Sheet Metal Forming (ed. Koistinen D. P. & Wang N.-M.), (1978), pp. 237-267, New York, Plenum press.
[12] V. Tvergaard, ZAMM 60 (1980), T26-T34.
[13] A. Needleman, V. Tvergaard, Appl. Mech. Rev. 45 (1992), S3-S18.
[14] J.L. Bassani, J.W. Hutchinson, K.W. Neal, IUTAM Symposium, Germany, (1978) 1-13.
[15] F. Barlat, Mat. Sci. Engng. 91 (1987), 55-72.
[16] J.W. Hutchinson, K.W. Neal, In Mechanics of Sheet Metal Forming (ed. Koistinen D. P. & Wang N.-M.), (1978), pp. 127-153, New York, Plenum press.
[17] V. Tvergaard, Int. J. Mech. Sci. 20 (1978), 651-658.
[18] D. Banabic, F. Barlat, O. Cazacu, T. Kuwabara, Int. J. Mater. Form. 3 (2010), 165-189.
[19] P.D. Wu, K.W. Neale, E. Van der Giessen, Proc. R. Soc. Lond. A 453 (1997), 1831-1848.
[20] K. Nakazima, T. Kikuma and K. Hasuka, Yawata Technical Report 264 (1968), 8517-8530.
[21] A. Graf, W.F. Hosford, Met. Trans., 24A (1993), 2503-2512.
[22] A. Graf and W. Hosford, Int. J. Mech. Sci., 36 (1994), 897-910.
[23] M. Gotoh, M., Int. J. Solids Struct. 21 (1985), 1149-1163.
[24] M. Kuroda, V. Tvergard, Int. J. Mech. Sci. 42 (2000), 867-887.

[25] R. Arrieux, C.Bedrin, M. Bovin, M., Proc. 12th IDDRG Congress (1982), pp. 61-71.
[26] I. Gronostajski, J. Mech. Work. Technol. 10 (1984), 349-362.
[27] T.B. Stoughton, Int. J. Mech. Sci. 42 (2000), 1-27.
[28] K. Yoshida, T .Kuwabara, K. Narihara, S. Takahashi, Int. J. Forming Processes 8 (2005), 283-298.
[29] T. Kuwabara, M. Ishiki, M. Kuroda, S. Takahashi, Journal de Physique IV 105 (2003), 347-354.
[30] T. Kuwabara, K. Yoshida, K. Narihara, S. Takahashi, Int. J. Plasticity 21 (2005), 101-117.
[31] K. Yoshida, T. Kuwabara, Int. J. Plasticity 23 (2007), 1260-1284.
[32] C. Teodosiu, Z. Hu, in: Shen, Dawson (Eds.), Proceedings of the 5th NUMIFORM Conference, Simulation of Materials Processing: Theory, Methods and Applications (1995), pp. 173-182.
[33] C. Teodosiu, Z. Hu, in: Carstensen J. V. Leffers T., Lorentzen T., Pedersen O. B., Sorensen B. F., Winther G. (Eds.), Proceedings of the 19th Riso International Symposium on Materials Science (1998), pp. 149-168.
[34] F. Barlat, J. Lian, Int. J. Plasticity 5 (1989), 51-66.
[35] R.W. Logan, W.F. Hosford, In. J. Mech. Sci. 22 (1980), 419-430.
[36] D. Peirce, R.J. Asaro, A. Needleman, Acta Metall. 31 (1983) 1951-1976.
[37] R.J. Asaro, A. Needleman, Acta Metall. 33 (1985) 923-953.
[38] A. Parmar, P.B. Melor, Int. J. Mech. Sci. 20 (1978), 385-391.
[39] J. Lian, F. Barlat, B. Baudelet, Int. J. Plasticity 5 (1989), 131-147.
[40] A. Graf, W.F. Hosford, Metall. Trans. A 21 (1990), 87-94.
[41] P.A. Friedman, J. Pan, Int. J. Mech. Sci. 42 (2000), 29-48.
[42] M. Kuroda, V. Tvergaard, Int. J. Solids Struct. 37 (2000), 5037-5059.
[43] Z. Marciniak, K. Kuczyński, T. Pokora, Int. J. Mech. Sci. 15 (1973), 789-805.
[44] J.W. Hutchinson, K.W. Neal, In Mechanics of Sheet Metal Forming (ed. Koistinen D. P. & Wang N.-M.), (1978), pp. 269-285, New York, Plenum press.
[45] A. Barata da Rocha, F. Barlat, J.M. Jalinier, Mat. Sci. Eng. 68 (1984), 151-164.
[46] T. Kuwabara, M. Umemura, K. Yoshida, M. Kuroda, J. JILM 56 (2006), 323-328. (in Japanese)
[47] R. Pearce, D. Ganguli, J. Inst. Metals 100 (1972), 289-295.
[48] S. Kohara, M. Katsuta, J. JILM 28 (1978) 277-283. (in Japnase)
[49] F. Barlat, J.C. Brem, J.W. Yoon, K. Chung, R.E. Dick, D.J. Lege, F. Pourboghrat, S.H. Choi, E. Chu, Int. J. Plasticity 19 (2003), 1297-1319.
[50] J.W. Yoon, F. Barlat, R.E. Dick, K. Chung, T.J. Kang, Int. J. Plasticity 20 (2004), 495-522.
[51] T. Kuwabara, S. Ikeda, T. Kuroda, J. Material Process. Technol. 80/81(1998), 517-523.
[52] M. Kuroda, V. Tvergaard, J. Mech. Phys. Solids 49 (2001), 1239-1263.
[53] M. Ishiki, T. Kuwabara, Y. Hayashida, Int. J. Mater. Forming 4 (2011), 193-204.
[54] F. Sugawara, T. Kuwabara, Proc. 62 nd Japanese Joint Conference for Technology of plasticity, Toyohashi, (2011), 177-178. (in Japanese)
[55] R. Hill, J.W. Hutchinson, J. Applied Mech. 59 (1992), S1-S9.
[56] R. Hill, S.S. Hecker, M.G. Stout, Int. J. Solids and Structures, 31(1994), 2999-3021.